ACS OMEGA

Open Access

This article is licensed under CC-BY-NC-ND 4.0

http://pubs.acs.org/journal/acsodf

Article

Sustainable Active Packaging from On-Demand Degradable PLA/PBAT and Zn-Doped TiO_2 Composites

Nattawut Yuntawattana,* Thanapat Buaban, and Teerapat Siri

Cite This: *ACS Omega* 2025, 10, 2931−2939

Read Online

ACCESS | Metrics & More | Article Recommendations | Supporting Information

ABSTRACT: Shelf life extendable packaging and ethylene scavenger technologies for climacteric fruits and vegetables have garnered much attention in recent years. These products effectively enable food quality to be maintained, ensure food safety, and prolong food storage life, which are key to helping reduce food waste. Current technologies − both in terms of academic research and broader commercial application − imply the use of chemicals that are of low activity, of high toxicity, or difficult to handle. Therefore, in this work, we prepared Zn-doped TiO_2 photocatalysts, containing 0.1 and 2.0 mol % of Zn dopant ($\mathbf{Zn_{0.1\%}}$-$\mathbf{TiO_2}$ and $\mathbf{Zn_{2\%}}$-$\mathbf{TiO_2}$), through a simple sol−gel method, which were then applied to be used as ethylene scavenger fillers in the preparation of on-demand degradable active packaging. TiO_2 particles were also prepared under identical conditions for comparison. The active composite film containing $\mathbf{Zn_{0.1\%}}$-$\mathbf{TiO_2}$ was shown to be a better active packaging than the one containing TiO_2 and was able to extend the shelf life of bananas for up to 8 days. In addition, the incorporation of Zn-doped TiO_2 particles did not significantly compromise either the mechanical properties of the polymer composite film or change its degradation behavior; it slightly improved the thermal stability. Moreover, the active composite film could be degraded on demand by immersing it into a 3 M KOH solution − leading to almost complete polymer film degradation after 4 h at room temperature. The developed active packaging model is a very promising candidate and could serve for future optimization as sustainable active food packaging.

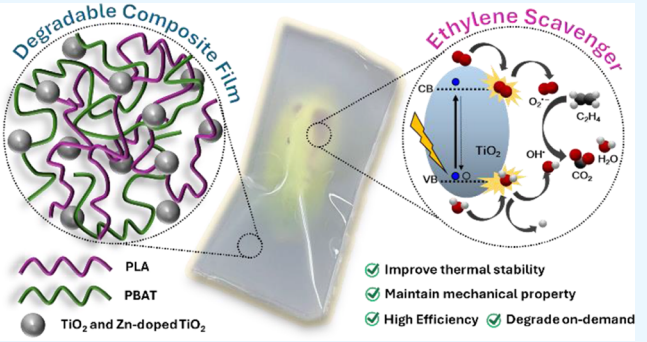

INTRODUCTION

There is enough food in the world to feed the global population, yet more than 600 million people are undernourished. Food waste is estimated by the Swedish Institute for Food and Biotechnology to be 1.3 billion tons per year − double of what is needed to feed the 600 million undernourished people.[1] The problem is therefore 2-fold. First, food production is carbon-intensive − it contributes up to 37% of global greenhouse gases.[2] Second, food production is unbalanced, leading to the situation described above whereby a surplus of food still leaves a significant proportion of humankind hungry.

To alleviate both of these problems, it would be beneficial to prolong the shelf life of fresh foods. In 2019, the Food and Agriculture Organization of the United Nations (FAO) reported that 14% of food produced for consumption worldwide was deteriorated and lost before even reaching the market.[1] Addressing this problem would enable production to be optimized, instead of being caught in a cycle of overproduction and waste, and thereby reduce the carbon intensity of the global food production system. Equally, a longer shelf life could enable food to be transported more viably to where it is needed.

A major factor in the type of food deterioration described above is ethylene. Ethylene, a gaseous phytohormone, controls the ripening process, maturation, and corruption of postharvest climacteric fruits and vegetables such as bananas, mangoes, apples, and tomatoes, etc. Even very low concentrations of ethylene (0.1−1 ppm) have been shown to ripen the fruits. Controlling ethylene concentration not only allows the extension of the shelf life but also maintains high quality and ensures the safety of postharvest climacteric produce.[3−5] There have been many strategies reported to control and scavenge the ethylene gas produced from climacteric fresh produce (Figure 1). For example, high surface area and porous materials such as zeolites,[6−8] metal−organic frameworks (MOFs),[9−11] and activated carbon[12,13] have been studied as ethylene adsorbers. The use of these physical ethylene adsorbents allows minimization and concentration control of

Received: October 7, 2024
Revised: December 25, 2024
Accepted: January 3, 2025
Published: January 16, 2025

© 2025 The Authors. Published by American Chemical Society

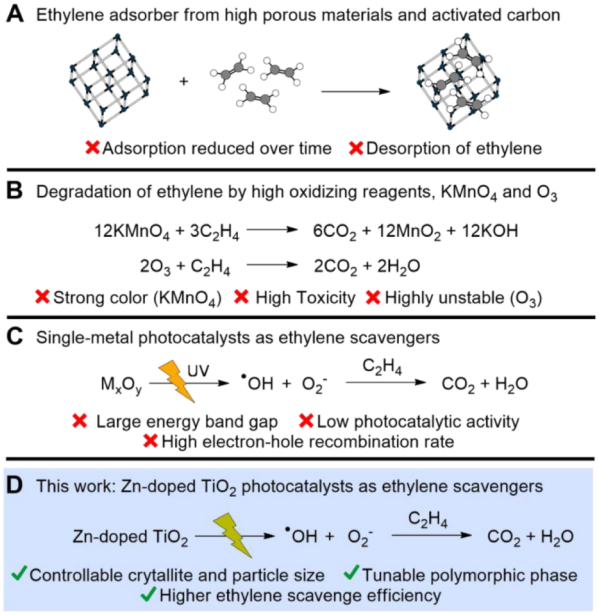

Figure 1. (A) Cartoon shows ethylene adsorption by high porous materials, (B) oxidation of ethylene by strong oxidizing agents, $KMnO_4$ and O_3, (C) degradation of ethylene by photocatalyst TiO_2, and (D) decomposition of ethylene by metal-doped TiO_2 photocatalyst.

ethylene gas in storage containers, leading to the extension of the shelf life of postharvest perishable fruits and vegetables. However, the adsorption ability of these ethylene adsorbents significantly decreases over time as they become saturated. Moreover, the adsorbed ethylene can also be released via a desorption mechanism since these materials only adsorb ethylene rather than decompose it.[11,14] Utilizing an ethylene gas decomposer is another approach that has garnered much attention. Among these, $KMnO_4$ is the most widely utilized ethylene scavenger due to its high oxidizing ability.[15−17] $KMnO_4$ is generally impregnated onto microporous mineral particles and packaged in small sachets to prevent direct food contact. The main limitations of $KMnO_4$ are its high toxicity and deep purple color, which make it difficult and unsuitable to apply for food applications.[15,18] Ozone (O_3) has also been reported to scavenge ethylene by reducing the activities of cell wall enzymes.[19] In addition, O_3 is considered a safe food additive according to the Food and Drug Administration (FDA). However, it is rather difficult to handle and highly unstable, leading to the formation of oxygen molecules and loss of ability to oxidize ethylene.[4,20]

Another strategy that has received much attention is to degrade ethylene under light by utilizing photocatalysts. This strategy has proven to show high efficiency and low energy consumption and is environmentally friendly. The most employed photocatalyst is TiO_2 due to its low toxicity, earth abundance, and inexpensive cost.[21−24] Upon photo irradiation, electrons (e^-) on the TiO_2 surface are activated and further produce highly reactive hydroxyl radicals and superoxide ions by reacting with hydroxide ions and water, respectively. These strong oxidizing species can then convert ethylene into carbon dioxide and water.[25] However, due to the large energy bandgap of TiO_2 (~3.0−3.2 eV), TiO_2 sometimes shows unacceptably low photocatalytic activity. Additionally, a high-energy light source, especially in the UV region (<380 nm wavelength), is required to activate TiO_2.[22,26] The requirement for UV activation of TiO_2 makes it impractical to use with food applications as certain food nutrients can be degraded upon exposure to UV light, which would further diminish the food quality.[27] There are several strategies reported to improve the photocatalytic activity of TiO_2, including controlling crystal structures and morphologies,[28−30] introducing defect,[31−33] and doping with metal and nonmetal elements.[34−36] Modification of TiO_2 by doping it with metal and nonmetal dopants is found to be one of the highly effective methods to enhance its photocatalytic activity. Particularly, several reports demonstrated that doping TiO_2 with a Zn dopant reduces the energy bandgap, minimizes the rate of electron−hole recombination, and tunes the crystal structure of TiO_2, thus resulting in enhanced photocatalytic performance.[36−39]

As can be seen from the summary above, the current state-of-the-art is not sufficiently advanced − in terms of both academic research and broader commercial application. In response, we envisioned that Zn-doped TiO_2 is a promising candidate to use as ethylene scavenger fillers in active packaging. To the best of our knowledge, there has been no report on using these particles as ethylene scavenger fillers in active packaging. Herein, we prepared Zn-doped TiO_2 particles with 0.1 and 2.0 mol % of Zn dopant. TiO_2 particles were also synthesized under the same conditions as a control. The prepared TiO_2 and Zn-doped TiO_2 were then incorporated into the PLA/PBAT blend films to make composite films by the solvent casting method, which were then studied as active packaging for bananas. The efficiencies of active packaging were evaluated by measuring the green color intensity, analyzing the percentage of browning area of the banana skin upon storage, as well as examining the banana mass loss and firmness. Combination effects between smaller particle and crystallite sizes and a higher anatase polymorph of Zn-doped TiO_2 were found to enhance the effectiveness of the model active packaging. The effects of metal oxide particles on thermal stability, mechanical property, as well as the degradation behavior of the composite films were also determined.

METHODS

Synthesis of TiO_2 Particles. TiO_2 particles were synthesized via a sol−gel method. First, $Ti(O^nBu)_4$ (10.6 g, 31.14 mmol) was filled in a 100 mL round-bottom flask equipped with a magnetic stir bead. Absolute ethanol (30 mL) was then added to the round-bottom flask, and the reaction solution was vigorously stirred at room temperature. A solution of deionized water (2.24 g, 0.12 mol) in EtOH (10 mL) was added dropwise into the stirred solution of $Ti(O^nBu)_4$ during which white precipitation was formed. The reaction mixture was then stirred at room temperature for 3 h. The white precipitation was then isolated using a centrifuge (UGAIYA, TG16-WS), washed with absolute ethanol (2 × 15 mL), and dried in a hot air oven at 50 °C for 20−24 h. The white precipitation was then calcined at 500 °C for 2 h using a heating rate of 10 °C/min to give a pale gray solid as a product.

Synthesis of Zn-Doped TiO_2 Particles ($Zn_{0.1\%}$-TiO_2 and $Zn_{2\%}$-TiO_2). All Zn-doped TiO_2 particles ($Zn_{0.1\%}$-TiO_2 and $Zn_{2\%}$-TiO_2) were synthesized by utilizing a similar preparation method to TiO_2 particles. Each Zn-doped TiO_2 particle possesses a general formulation of $Zn_{x\%}$-TiO_2 where x represents mol % of $Zn(CH_3COO)_2{\cdot}2H_2O$ used in the preparation of Zn-doped TiO_2 compared to $Ti(O^nBu)_4$.

https://doi.org/10.1021/acsomega.4c09138
ACS Omega 2025, 10, 2931−2939

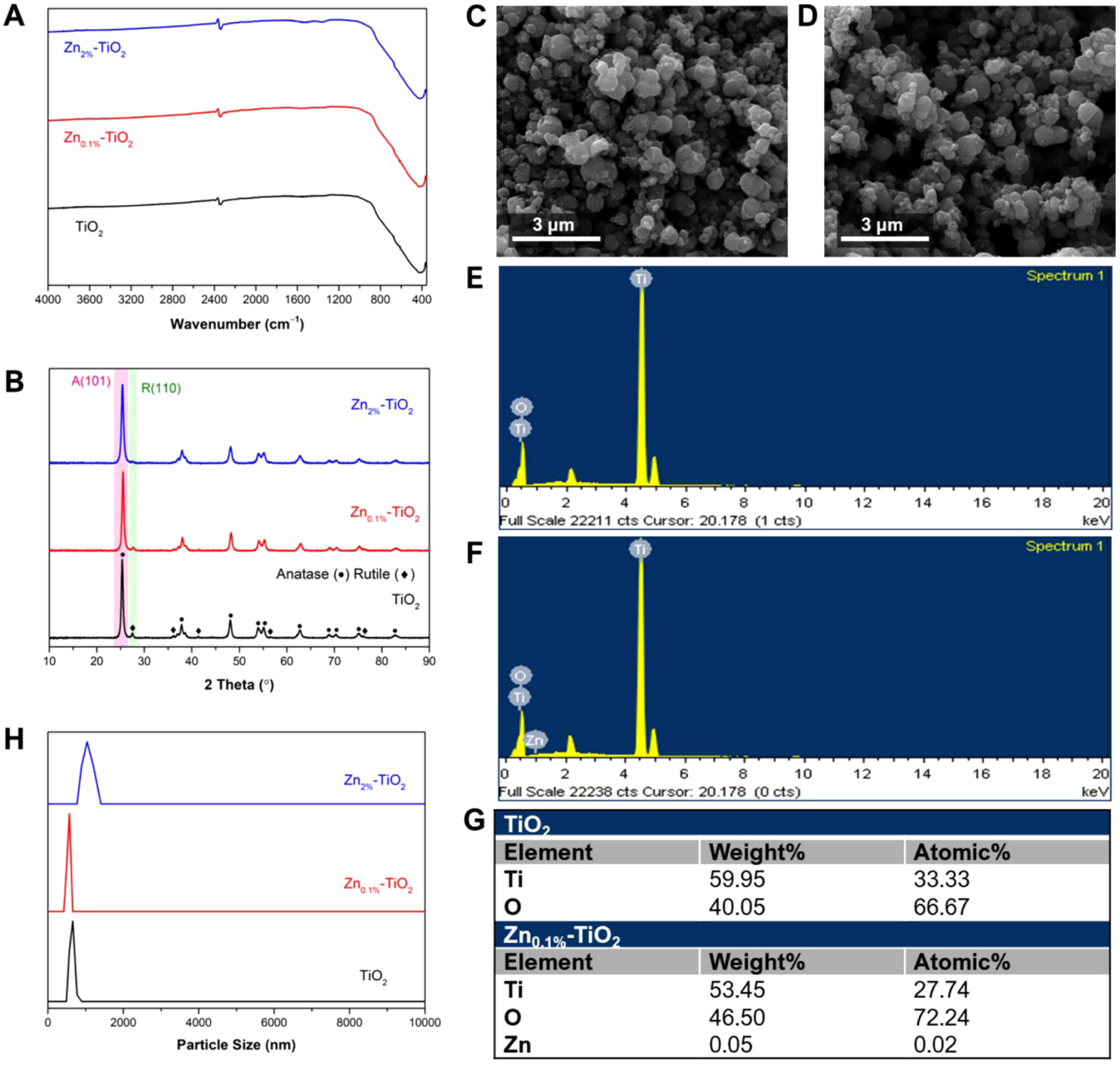

G

TiO2		
Element	Weight%	Atomic%
Ti	59.95	33.33
O	40.05	66.67
Zn0.1%-TiO2		
Element	Weight%	Atomic%
Ti	53.45	27.74
O	46.50	72.24
Zn	0.05	0.02

Figure 2. Characterizations of TiO_2 and Zn-doped TiO_2. (A) Stacked FTIR spectra, (B) stacked powder XRD diffractograms, (C) SEM photograph of TiO_2, (D) SEM photograph of **$Zn_{0.1\%}$-TiO_2**, (E) SEM-EDS spectrum of TiO_2, (F) SEM-EDS spectrum of **$Zn_{0.1\%}$-TiO_2**, (G) chemical composition analysis results from SEM-EDS of TiO_2 and **$Zn_{0.1\%}$-TiO_2**, and (H) stacked DLS spectra of TiO_2 and Zn-doped TiO_2 particles.

First, $Ti(O^nBu)_4$ (10.6 g, 31.14 mmol) was filled in a 100 mL round-bottom flask equipped with a magnetic stir bead. Absolute ethanol (30 mL) was then added to the round-bottom flask, and the reaction solution was vigorously stirred at room temperature. A solution of deionized water (2.24 g, 0.12 mol) in EtOH (10 mL), containing different amounts of $Zn(CH_3COO)_2{\cdot}2H_2O$ depending on the type of Zn-doped TiO_2, was then added dropwise to the reaction mixture, during which white precipitation was formed. $Zn(CH_3COO)_2{\cdot}2H_2O$ (6.84 mg, 0.03 mmol) and $Zn(CH_3COO)_2{\cdot}2H_2O$ (0.14 g, 0.62 mmol) were used for the preparation of **$Zn_{0.1\%}$-TiO_2** and **$Zn_{2\%}$-TiO_2**, respectively. The reaction mixture was allowed to be vigorously stirred at room temperature for 3 h. The white precipitation was then isolated using a centrifuge (UGAIYA, TG16-WS), washed with absolute ethanol (2 × 15 mL), and dried in a hot air oven at 40 °C for 120−144 h. The white precipitation was then calcined at 500 °C for 2 h using a heating rate of 10 °C/min to give light gray solids as products.

Preparation of Polymer and Polymer Composite Films. All of the polymer films (**P1**−**P4**) were prepared by a solvent casting process. In the case of the pristine polymer film (**P1**), PLA (5.40 g, 90 wt %) and PBAT (0.60 g, 10 wt %) were dissolved in DCM (113 mL) and allowed to stir at room temperature for 2 h or until all the polymer was fully dissolved. The polymer solution was then transferred to a PTFE-coated aluminum mold (19.5 × 19.5 cm). The mold was covered with aluminum foil and left at room temperature for 18−20 h to allow the solvent to evaporate. The polymer film was then

https://doi.org/10.1021/acsomega.4c09138
ACS Omega 2025, 10, 2931−2939

taken out of the mold and dried in a hot air oven at 40 °C for 120−144 h prior to further characterizations. For polymer composite films (**P2−P4**), the preparation method was similar to that of the pristine polymer film except in the first step. After the polymers were fully dissolved, the prepared TiO_2 or Zn-doped TiO_2 (1.20 g, 2 wt %) was added to the stirred polymer solution before the solution mixture was transferred to a PTFE-coated aluminum mold.

Application of the Prepared Polymer Composite Film as an Active Packaging Study. The prepared polymer (**P1**) and polymer composite (**P2−P4**) films were used to make small pouches to package fresh bananas. First, the prepared polymer and polymer composite films were cut into a square shape with dimensions of 17 × 17 cm. The polymer film was then half-folded to make a rectangle-shaped pouch in which the edges of the pouch were sealed together using heat. Five fresh bananas of similar size and ripeness level were selected, cleaned with DI water, and dried. The fresh bananas were then packaged in the prepared pouches, while an unpackaged banana was used as a control sample. The packaged bananas and the control banana sample were left under light exposure at room temperature. Each banana sample was then monitored and photographed every 2 days for 10 days to monitor the change in skin color. The change in skin color was then analyzed in terms of green color intensity and browning area using the ImageJ program.

Shelf life extension experiments were also repeated to ensure the reliability of the study. In these repeated analyses, 15 fresh bananas with similar sizes and ripeness levels were used. These bananas were divided into five groups of three bananas each. One group of three bananas was used as a control group, and then, the four other groups of three bananas were packaged into different pouches (18 × 24 cm). For each group of three bananas, two of them were photographed every 2 days for 10 days to observe the change of skin color, which was later analyzed by the ImageJ program in terms of green color intensity reduction and percentage of browning area. The remaining banana in each group was used to analyze firmness and mass loss after 6 days of storage. For the firmness analysis, a penetrometer model FT327 (TR, Italy) with a tip size of 3 mm (1/8 in.) was used.

On-Demand Degradation Study of the Prepared Polymer and Polymer Composite Films. The predried polymer (**P1**) and polymer composite (**P2−P4**) films were cut into a square shape with dimensions of 30 × 30 mm. The weight of each film was then measured and recorded as the initial weight of the polymer film (W_i). A 3 M solution of KOH (30 mL) was prepared in a 100 mL beaker. The polymer and polymer composite films were then immersed in the prepared KOH solution and allowed to vigorously stir at ambient temperature for 4 h. The remaining polymer and polymer composite films were then collected, rinsed with DI water (10 mL × 3), and dried in a hot air oven. The dried polymer and polymer composite film residues were then weighed and recorded as the weight of the polymer film after degradation at 4 h (W_t). The degradation rate of the polymer and polymer composite was then determined in terms of percent mass loss (% mass loss) by using eq 1.

$$\%\ \text{mass loss} = \frac{W_i - W_t}{W_i} \times 100\% \quad (1)$$

RESULTS AND DISCUSSION

Synthesis and Characterization of TiO_2 and Zn-Doped TiO_2 Particles. TiO_2 and Zn-doped TiO_2 (**$Zn_{0.1\%}$-TiO_2** and **$Zn_{2\%}$-TiO_2**) were synthesized by a sol−gel method since it is a fast and straightforward means to prepare various types of metal oxide particles under mild conditions.[40] After calcination at 500 °C for 2 h, an off-white solid was obtained as a product. The chemical compositions of TiO_2 and Zn-doped TiO_2 were analyzed by ATR-FTIR (Figure 2A). TiO_2 and Zn-doped TiO_2 showed a clear characteristic absorption band around 425 cm^{-1}, which is assigned to the Ti−O stretching vibration.[41] The lack of a broad absorption band around 3400 cm^{-1} (−OH stretching vibration) and an absorption band around 1600 cm^{-1} (Ti−OH bending vibration) suggested the absence of water molecules inside or at the surface of TiO_2 and Zn-doped TiO_2 particles. Moreover, the disappearance of additional peaks in Zn-doped TiO_2 indicated efficient dispersion of the Zn dopant in TiO_2 and the absence of Zn clusters in TiO_2 structure, which is in good agreement with powder X-ray diffraction (XRD) analysis.[42] Powder XRD measurement confirmed the successful formation and was used to identify the polymorphic phase of the TiO_2 and Zn-doped TiO_2 particles (Figure 2B). TiO_2 exhibited two different sets of diffraction signals, which belong to the two distinct TiO_2 polymorphs, namely, anatase and rutile. The major diffraction signals represented the anatase polymorph according to JCPDS 75−1537, whereas a set of minor diffraction peaks at 2θ of 27.48° (110), 36.15° (101), 41.35° (111), 56.69° (220), and 75.99° (202) were attributed to the rutile polymorph.[43] Analysis of the ratio between the two highest intensity signals for anatase (101) and rutile (110) using the Spurr−Myers equation suggested the formation of around 93% anatase polymorph for TiO_2.[44] Interestingly, the addition of Zn dopants resulted in an increase in the formation of the TiO_2 anatase phase, as evidenced by a decrease in diffraction signal intensities of the rutile polymorph (∼94% anatase for **$Zn_{0.1\%}$-TiO_2** and ∼95% anatase for **$Zn_{2\%}$-TiO_2**). A similar behavior was also observed when CuO was used as a dopant for TiO_2 by Pillai and Nolan.[45] This might be explained by enhanced stabilization of the TiO_2 anatase phase over the rutile polymorph by the addition of the Zn dopant. The crystallite size (D) of TiO_2 and Zn-doped TiO_2 was evaluated by Scherrer's equation using the highest intensity diffraction peak ((101) lattice plane) of the anatase polymorph.[46] TiO_2 demonstrated a bigger crystallite size of 17.08 nm, while the addition of 0.1 mol % of Zn dopant resulted in the formation of TiO_2 nanoparticles with a slightly smaller crystallite size (D = 16.43 nm). Increasing the amount of Zn dopant to 2 mol % further decreased the crystallite size to 12.56 nm. The disappearance of diffraction signals corresponding to Zn or ZnO indicated a good dispersion of Zn dopants in TiO_2, which agreed well with the FTIR analysis.[22] SEM was utilized to analyze particle morphology, and spherical-shaped particles were observed in all cases (Figures 2C,D and S1). Additionally, SEM-EDS suggested that the ratio of Ti and O was very close to 1:2, indicating the formation of TiO_2 particles (Figure 2E). The presence of a Zn dopant in **$Zn_{0.1\%}$-TiO_2** and **$Zn_{2\%}$-TiO_2** particles was also confirmed by SEM-EDS (Figures 2F and S1). However, a slightly lower atom percent compared with the actual amount of the used Zn precursor was observed (Figures 2G and Table S1).

https://doi.org/10.1021/acsomega.4c09138
ACS Omega 2025, 10, 2931−2939

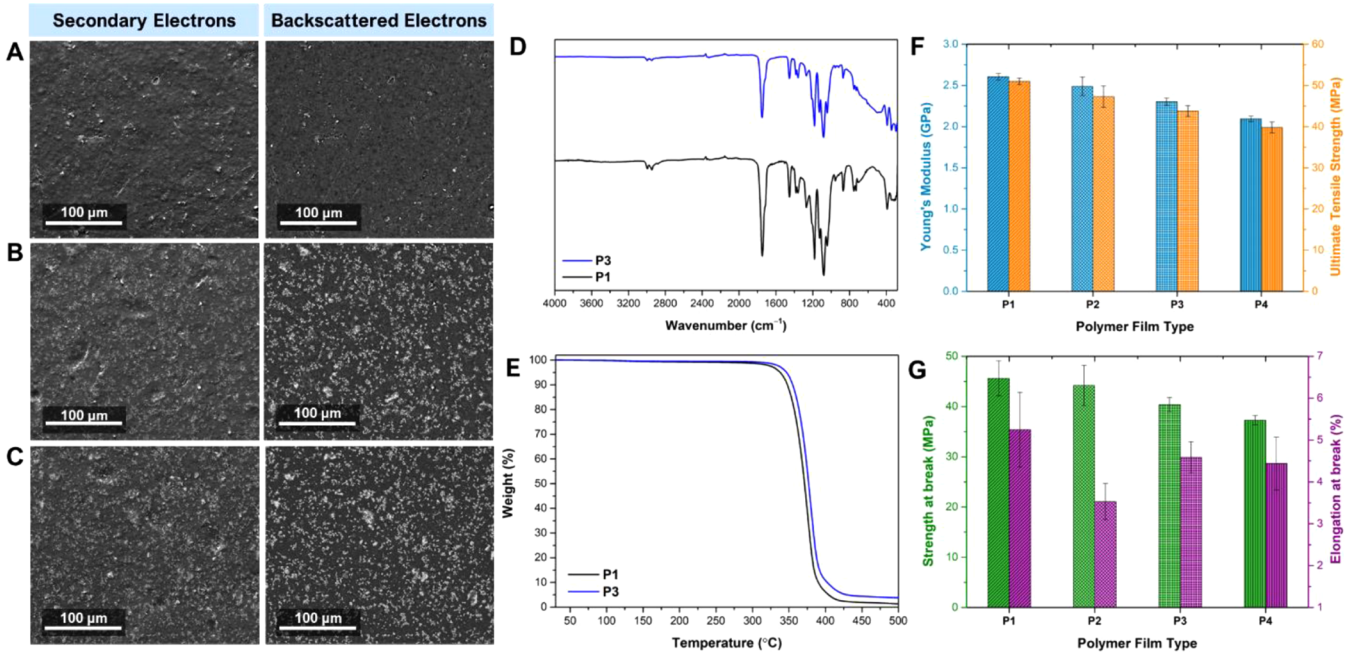

Figure 3. Characterizations of polymer and polymer composite films (**P1**−**P4**): Backscattered electrons and secondary electrons SEM images of (A) **P1**, (B) **P2**, (C) **P3**, (D) FTIR spectra of polymer (**P1**) vs polymer composite (**P3**) films, (E) TGA thermogram of polymer (**P1**) vs polymer composite (**P3**) films, (F) plots of Young's modulus and ultimate tensile strength of different polymer films, and (G) bar charts show strength at break and elongation at break of all polymer films.

The particle sizes of TiO_2 and Zn-doped TiO_2 in the solid state were examined using SEM. After a careful analysis using ImageJ, TiO_2 revealed an average particle size of 672.0 ± 53.16 nm, while **$Zn_{0.1\%}$-TiO_2** exhibited a slightly smaller average particle size of 656.4 ± 91.74 nm. Increasing the Zn dopant to 2 mol % resulted in a further reduction in the particle size to 609.4 ± 40.65 nm. DCM was used as a solvent in the preparation of polymer films. To understand the particle size and aggregation behavior of particles in solution, the particle sizes of TiO_2 and all Zn-doped TiO_2 in DCM solution were examined using a Zeta sizer (Figure 2H). The results demonstrated that TiO_2 possessed a particle size in DCM around 655.4 ± 26.86 nm, while **$Zn_{0.1\%}$-TiO_2** exhibited an average particle size of 542.9 ± 11.77 nm. In contrast, a much larger particle size of 1000.6 ± 70.32 nm was observed for **$Zn_{2\%}$-TiO_2**. The latter suggested that there might be some degree of aggregation of **$Zn_{2\%}$-TiO_2** particles in the DCM solution.

Preparation and Characterization of Polymer and Polymer Composite Films. Control polymer film (**P1**) was prepared from a pristine PLA/PBAT blend, while polymer composite films (**P2**−**P4**) were prepared from the successfully synthesized TiO_2, **$Zn_{0.1\%}$-TiO_2**, and **$Zn_{2\%}$-TiO_2** respectively, and PLA/PBAT blend via a solvent casting process using DCM as a solvent. The prepared polymer and polymer composite films were then characterized by various techniques. First, the surface morphology of all the polymer films (**P1**−**P4**) and the dispersion of TiO_2 and Zn-doped TiO_2 particles in the polymer composite films were examined by SEM. Secondary electrons SEM micrographs demonstrated that the pristine PLA/PBAT blend film (**P1**) possessed a smooth surface, suggesting good miscibility between PBAT and PLA (Figure 3A). This agrees with the observation of a single decomposition behavior in TGA analysis. As expected, the incorporation of TiO_2 and Zn-doped TiO_2 into the PLA/PBAT blend film resulted in increased surface roughness of the composite films (Figures 3B,C and S2). Moreover, backscattered electron SEM images suggested a good dispersion of TiO_2 and Zn-doped TiO_2 in the composite films, even though some small aggregations of TiO_2 and Zn-doped TiO_2 particles were observed. This could be explained by stronger adhesion interaction between metal oxide nanoparticles than that of the cohesive force between metal oxide nanoparticles and the polymer matrix, which is confirmed by the shifting of FTIR signals of polymer composite films.

ATR-FTIR spectroscopy was utilized to study the chemical structure of polymer films and interactions between TiO_2 or Zn-doped TiO_2 particles with the polymer matrix (Figures 3D and S3). For the pristine polymer film (**P1**), a strong absorption band at 1749 cm^{-1} was observed, representing a stretching vibration of −C═O. Additionally, **P1** exhibited two absorption signals at 1180 and 1082 cm^{-1}, which were assigned to −C−O stretching vibrations of C−CO−O and O−C−CO, respectively.[47] The appearance of a single −C═O stretching band suggested the interaction between PLA and PBAT.[48] In the case of polymer composite films (**P2**−**P4**), similar FTIR spectra to that of the pristine polymer film were obtained, except for the presence of a broad absorption band around 450−460 cm^{-1}, which was attributed to the Ti−O stretching vibration. The latter suggested the insignificant change in the chemical structures of both PLA and PBAT upon the addition of TiO_2 and Zn-doped TiO_2 particles. Both −C═O (1751−1753 cm^{-1}) and −Ti−O stretching bands shifted to higher wavenumbers, compared with those observed in the pristine polymer film and TiO_2 or Zn-doped TiO_2 particles alone, respectively. However, absorption band shifting was not observed for −C−O stretching vibrations in either the C−CO−O or the O−C−CO. This suggested the interaction of TiO_2 or Zn-doped TiO_2 with the −C═O functional group of the PLA/PBAT matrix.

https://doi.org/10.1021/acsomega.4c09138
ACS Omega 2025, 10, 2931−2939

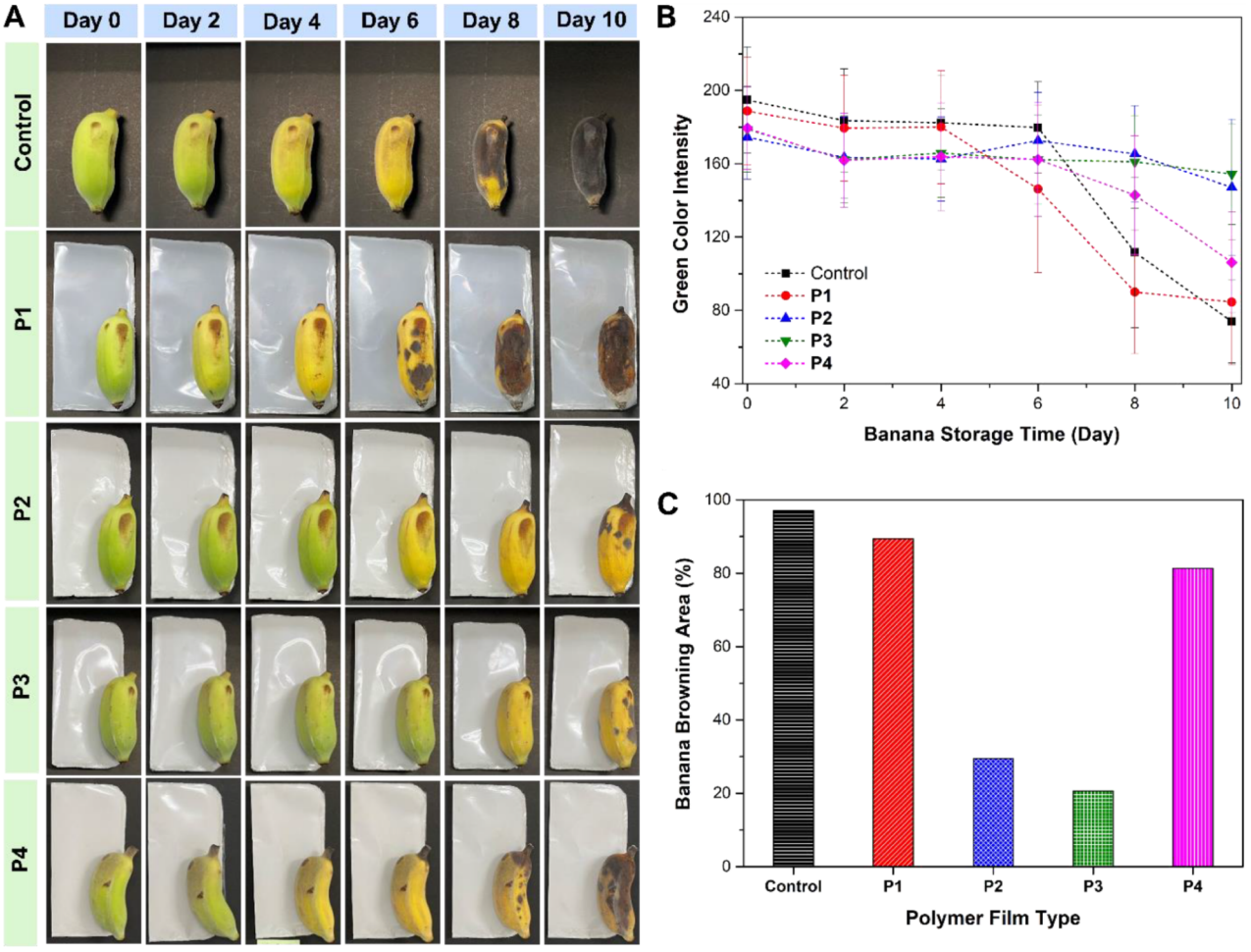

Figure 4. Efficiency evaluation of polymer and polymer composite films in prolonging the shelf life of bananas: (A) control banana samples vs banana packaged in different polymer (**P1**) and polymer composite (**P2**−**P4**) films, (B) green color intensity analysis of the banana skin, (C) analysis of the browning area of the banana skin after 10 days of storage.

Thermal and Mechanical Properties of Polymer and Polymer Composite Films. Thermal stabilities of the pristine polymer (**P1**) and polymer composite (**P2**−**P4**) films were evaluated by TGA (Figures 3E and S4). The samples were heated from 25 to 500 °C with a heating rate of 10 °C/min, and polymer mass losses were measured as a function of temperature. In all cases, a single decomposition profile was observed, indicating the homogeneity of the polymer films. The absence of sample mass loss at the beginning of the measurement (T = 25−110 °C) suggested the disappearance of water and solvent molecules in all the polymer films. **P1** shows a decomposition temperature at five percent mass loss (T_{d5}) of 338 °C, while slightly higher T_{d5} compared to the pristine polymer film was observed for polymer composite films **P2** and **P3** (T_{d5} = 342 and 347 °C for **P2** and **P3**, respectively). The latter suggested that the incorporation of metal oxide particles slightly improved polymer film thermal stability, which might be due to the interaction between metal oxide nanoparticles and the polymer matrix. It should be noted, however, that **P4** exhibited a very similar T_{d5} to that of **P1** (Figure S4 and Table S2). In addition, all of the polymer composite films were physically transparent (Figure S5).

Mechanical properties of the pristine polymer (**P1**) and polymer composite (**P2**−**P4**) films were analyzed by tensile testing (Figures 3F,G and S6). The samples were prepared and measured according to ASTM D882, and the data are listed in Table S3. Standard deviations were calculated from triplicate samples. Overall, the incorporation of 2 wt % of TiO_2 or Zn-doped TiO_2 into the PLA/PBAT blend film did not significantly compromise the mechanical properties of the polymer composite films. The pristine PLA/PBAT film (**P1**) showed an ultimate tensile strength of 51.0 ± 0.8 MPa and a tensile strength at break of 45.6 ± 3.5 MPa, while a Young's modulus of 2.60 ± 0.04 GPa and an elongation at break of 5 ± 0.9% were obtained. Polymer composite films (**P2**−**P4**) showed a similar ultimate tensile strength, tensile strength at break, and elongation at break, while a slightly lower Young's modulus compared to the pristine polymer film was observed.

Application of Polymer and Polymer Composite Films in Active Packaging. The application of polymer films as active packaging was investigated using bananas as a fruit model because they are climacteric fruits, showing clear color changes during the ripening process and an appropriate time frame in the deterioration process (Figure 4A). Green bananas with similar sizes and ripeness levels were selected and packaged into pouches prepared from pristine polymer (**P1**) and polymer composite (**P2**−**P4**) films. An unpackaged banana was also used as a control. The control banana and the packaged banana samples were then left under light

https://doi.org/10.1021/acsomega.4c09138
ACS Omega 2025, 10, 2931−2939

exposure at ambient temperature and monitored every 2 days for 10 days. One factor determining the ripeness of bananas is the change of the banana skin color from green to yellow and then brown, thanks to the decomposition of chlorophyll.[49] In general, bananas packaged in pouches made from composite films showed extended shelf life compared to the unpackaged banana. On the contrary, the banana packaged in pristine polymer film (**P1**) exhibited shorter storage life than the control sample, leading to browning of the banana skin on day 6. One possible explanation for this is that the ethylene gas released from the banana was kept inside the pouch without degrading, thus accelerating the ripening process of the banana. Analysis of green color intensity from the RGB color system using ImageJ allowed the determination of ripening and deterioration rates of bananas (Figure 4B). It was found that in all cases, the green color value was steady at the beginning of the test and started to decline after 4−8 days upon storage, depending on the samples. The banana packaged in the pristine polymer film (**P1**) exhibited a strip decline of green color intensity after day 4, while the control sample did not show a sharp reduction of green color value until day 6. Bananas packaged in the TiO_2 composite film (**P2**) showed extended shelf life and did not exhibit a decrease of green color intensity until day 6 upon storage. Interestingly, the banana packaged in the **$Zn_{0.1\%}$-TiO_2** composite film (**P3**) demonstrated the longest shelf life, which did not significantly change the green color intensity of the skin until day 8. This is almost twice as long as that of the banana packaged with the pristine polymer (**P1**) and slightly longer than that of the one packaged with **P2**. In the case of bananas packaged in the **$Zn_{2\%}$-TiO_2** composite film (**P4**), the banana skin showed a drastic drop of green color intensity on day 6. ImageJ also allowed analyzing the percentage of browning area of each banana sample (Figure 4C). The percentage of browning area of all the bananas after 10 days of storage was examined. Both the control sample and the banana packaged with the pristine polymer film (**P1**) showed 97% and 89% browning area, respectively. In contrast, a significant reduction of browning area was observed for the banana packaged with the TiO_2 composite film (**P2**), and only 29% browning area was found. In the case of bananas packaged with **$Zn_{0.1\%}$-TiO_2** composite films, **P3** showed 21% browning areas. This confirmed the ability to extend the shelf life of bananas and again agreed well with the green color intensity analysis. The banana packaged in the **$Zn_{2\%}$-TiO_2** composite film **P4**, however, exhibited around 81% browning area. The higher efficiency of the composite film incorporating **$Zn_{0.1\%}$-TiO_2** (**P3**) in extending the shelf life of bananas might be due to the synergistic effect between the smaller average particle size, crystallite size, and higher percent of anatase polymorph of the **$Zn_{0.1\%}$-TiO_2** particles.

To ensure the reliability of the shelf life extension analysis, a repeated experiment was performed with 15 fresh bananas. These bananas were divided into five groups of three bananas each. One group was used as a control, and then, the four other groups were packaged into different pouches made from polymer (**P1**) and different polymer composite films (**P2**−**P4**). Two banana samples in each group were monitored and photographed every 2 days for 10 days to observe the change of green color intensity and percentage browning area of the banana skin (Figures S7−S9). The remaining banana in each group was used to analyze firmness and mass loss upon 6 days of storage (Figure S10).

After a careful analysis of both green color intensity and percentage browning area of banana skin using the ImageJ program, some variation compared to the first test was observed. This can be expected due to the natural variation between individual bananas across the two experiments. However, firmness analysis as well as mass loss determination of banana samples after a 6-day storage confirmed the longest shelf life extension of a banana packaged in **P3** (Figure S10). The highest firmness of around 35 N was observed, which was almost 130% higher than that of a control banana sample (firmness ∼ 27 N). Mass loss measurement also suggested that bananas packaged in polymer composite films **P2**−**P4** exhibited a significantly lower mass loss of less than 4% compared to almost 20% mass loss for a control sample, suggesting shelf life extension of bananas packaged in the developed composite films. It should, however, be noted that there is no significant difference of mass loss observed in banana samples packaged in polymer (**P1**) and different polymer composite (**P2**−**P4**) films.

On-Demand Degradation Study of Polymer and Polymer Composite Films. Additionally, degradation studies of pristine polymer film (**P1**) and polymer composite films (**P2**−**P4**) were carried out in a 3 M aqueous solution of KOH for 4 h (Figure S11). Under these conditions , **P1**, **P3**, and **P4** exhibited nearly complete degradation − i.e., the films showed more than 88% mass loss. In contrast, the composite film **P2** showed a slightly slower degradation, 80% mass loss. The latter suggested that the incorporation of TiO_2 and Zn-doped TiO_2 did not significantly affect the degradation behavior of the polymer films.

CONCLUSIONS

In the present study, TiO_2 and two Zn-doped TiO_2 particles were successfully synthesized and characterized. The amount of Zn dopant was found to influence particle size, crystallite size, polymorphic phase, and aggregation behavior in DCM. The prepared TiO_2 and Zn-doped TiO_2 particles were then studied as ethylene scavenger fillers in the degradable PLA/PBAT composite films. A uniform dispersion of the fillers and their interactions with the polymer matrix were confirmed by SEM and FTIR, respectively. The incorporation of TiO_2 and Zn-doped TiO_2 slightly improved the thermal stabilities and did not seriously compromise the mechanical properties of the polymer composite films. The developed composite films containing 2 wt % of either TiO_2 or Zn-doped TiO_2 were shown to extend the shelf life of bananas compared to the pristine polymer film. In addition, the polymer composite containing **$Zn_{0.1\%}$-TiO_2** was found to possess higher efficiency as an active packaging to prolong the storage life of bananas than the one incorporating TiO_2. This might be explained by the synergistic effects between the smaller average particle size, crystallite size, and improved anatase polymorph of the **$Zn_{0.1\%}$-TiO_2** compared to TiO_2. Moreover, all the polymer composite films could be degraded on demand by immersing them in a 3 M KOH aqueous solution. The work presented in this paper therefore addresses deficiencies with previously reported solutions, with the developed composite films proving to be a promising solution. These could serve as the basis for future optimizations to use as sustainable active packaging for various types of food preservation.

https://doi.org/10.1021/acsomega.4c09138
ACS Omega 2025, 10, 2931−2939

■ ASSOCIATED CONTENT

Supporting Information

The Supporting Information is available free of charge at https://pubs.acs.org/doi/10.1021/acsomega.4c09138.

Details of materials and instruments, additional characterization data for the prepared metal oxide particles and polymer and polymer composite films, additional experimental results including the application of polymer and polymer composite films in active packaging and on-demand degradation study (PDF)

■ AUTHOR INFORMATION

Corresponding Author

Nattawut Yuntawattana − *Department of Materials Science, Faculty of Science, Kasetsart University, Bangkok 10900, Thailand;* orcid.org/0000-0002-3839-6149; Email: nattawut.yu@ku.th, fscinwy@ku.ac.th

Authors

Thanapat Buaban − *Department of Education, Faculty of Education, Kasetsart University, Bangkok 10900, Thailand*

Teerapat Siri − *Department of Materials Science, Faculty of Science, Kasetsart University, Bangkok 10900, Thailand*

Complete contact information is available at: https://pubs.acs.org/10.1021/acsomega.4c09138

Author Contributions

The manuscript was written through contributions of all authors. All authors have given approval to the final version of the manuscript.

Funding

Kasetsart University Research and Development Institute (Grant No. YF(KU)12.66)

Notes

The authors declare no competing financial interest.

■ ACKNOWLEDGMENTS

Kasetsart University Research and Development Institute (Grant No. YF(KU)12.66) was acknowledged for the financial support of this project. We also thank Mr. Paul C. Sanderson for valuable discussions and proofreading.

■ ABBREVIATIONS

FAO, the Food and Agriculture Organization of the United Nations; ppm, parts per million; MOF, metal−organic framework; FDA, Food and Drug administration; UV, ultraviolet; ATR-FTIR, attenuated total reflectance Fourier transform infrared; XRD, X-ray diffraction; JCPDS, Joint Committee on Powder Diffraction Standards; SEM, scanning electron microscope; EDS, energy-dispersive X-ray spectroscopy; DCM, dichloromethane; PLA, polylactide; PBAT, poly(butylene adipate-*co*-terephthalate)

■ REFERENCES

(1) FAO. *The State of Food and Agriculture 2019. Moving forward on food loss and waste reduction*; FAO: Rome, Italy, 2019.

(2) Rosenzweig, C.; Mbow, C.; Barioni, L. G.; Benton, T. G.; Herrero, M.; Krishnapillai, M.; Liwenga, E. T.; Pradhan, P.; Rivera-Ferre, M. G.; Sapkota, T. Climate change responses benefit from a global food system approach. *Nat. Food* **2020**, *1* (2), 94−97.

(3) Esser, B.; Schnorr, J. M.; Swager, T. M. Selective Detection of Ethylene Gas Using Carbon Nanotube-based Devices: Utility in Determination of Fruit Ripeness. *Angew. Chem., Int. Ed.* **2012**, *51* (23), 5752−5756.

(4) Wei, H.; Seidi, F.; Zhang, T.; Jin, Y.; Xiao, H. Ethylene scavengers for the preservation of fruits and vegetables: A review. *Food Chem.* **2021**, *337*, 127750.

(5) Zhang, J.; Cheng, D.; Wang, B.; Khan, I.; Ni, Y. Ethylene Control Technologies in Extending Postharvest Shelf Life of Climacteric Fruit. *J. Agric. Food Chem.* **2017**, *65* (34), 7308−7319.

(6) Marzano-Barreda, L. A.; Yamashita, F.; Bilck, A. P. Effect of biodegradable active packaging with zeolites on fresh broccoli florets. *J. Food Sci. Technol.* **2021**, *58* (1), 197−204.

(7) Soares, T. R. P.; Reis, A. F.; dos Santos, J. W. S.; Chagas, E. G. L.; Venturini, A. C.; Santiago, R. G.; Bastos-Neto, M.; Vieira, R. S.; Carvalho, R. A.; da Silva, C. F. NaY-Ag Zeolite Chitosan Coating Kraft Paper Applied as Ethylene Scavenger Packaging. *Food Bioprocess Technol.* **2023**, *16* (5), 1101−1115.

(8) Tzeng, J.-H.; Weng, C.-H.; Huang, J.-W.; Shiesh, C.-C.; Lin, Y.-H.; Lin, Y.-T. Application of palladium-modified zeolite for prolonging post-harvest shelf life of banana. *J. Sci. Food Agric.* **2019**, *99* (7), 3467−3474.

(9) Li, H.; Shi, L.; Li, C.; Fu, X.; Huang, Q.; Zhang, B. Metal−Organic Framework Based on α-Cyclodextrin Gives High Ethylene Gas Adsorption Capacity and Storage Stability. *ACS Appl. Mater. Interfaces* **2020**, *12* (30), 34095−34104.

(10) Zhang, B.; Luo, Y.; Kanyuck, K.; Bauchan, G.; Mowery, J.; Zavalij, P. Development of Metal−Organic Framework for Gaseous Plant Hormone Encapsulation To Manage Ripening of Climacteric Produce. *J. Agric. Food Chem.* **2016**, *64* (25), 5164−5170.

(11) Zhang, Y.; Yuan, S.; Chen, X.; Chen, M.; Sun, B.; Kim, D.; Yam, K. Potential of metal-organic frameworks to adsorb ethylene for fresh produce active packaging applications. *Food Packag. Shelf Life* **2023**, *35*, 101034.

(12) Abe, K.; Watada, A. E. Ethylene Absorbent to Maintain Quality of Lightly Processed Fruits and Vegetables. *J. Food Sci.* **1991**, *56* (6), 1589−1592.

(13) Bailén, G.; Guillén, F.; Castillo, S.; Serrano, M.; Valero, D.; Martínez-Romero, D. Use of Activated Carbon inside Modified Atmosphere Packages To Maintain Tomato Fruit Quality during Cold Storage. *J. Agric. Food Chem.* **2006**, *54* (6), 2229−2235.

(14) Chopra, S.; Dhumal, S.; Abeli, P.; Beaudry, R.; Almenar, E. Metal-organic frameworks have utility in adsorption and release of ethylene and 1-methylcyclopropene in fresh produce packaging. *Postharvest Biol. Technol.* **2017**, *130*, 48−55.

(15) Ozdemir, M.; Floros, J. D. Active Food Packaging Technologies. *Crit. Rev. Food Sci. Nutr.* **2004**, *44* (3), 185−193.

(16) Tirgar, A.; Han, D.; Steckl, A. J. Absorption of Ethylene on Membranes Containing Potassium Permanganate Loaded into Alumina-Nanoparticle-Incorporated Alumina/Carbon Nanofibers. *J. Agric. Food Chem.* **2018**, *66* (22), 5635−5643.

(17) Wang, C.; Ajji, A. Development of a novel ethylene scavenger made up of pumice and potassium permanganate and its effect on preservation quality of avocados. *J. Food Eng.* **2022**, *330*, 111101.

(18) Álvarez-Hernández, M. H.; Martínez-Hernández, G. B.; Avalos-Belmontes, F.; Castillo-Campohermoso, M. A.; Contreras-Esquivel, J. C.; Artés-Hernández, F. Potassium Permanganate-Based Ethylene Scavengers for Fresh Horticultural Produce as an Active Packaging. *Food Eng. Rev.* **2019**, *11* (3), 159−183.

(19) Minas, I. S.; Tanou, G.; Belghazi, M.; Job, D.; Manganaris, G. A.; Molassiotis, A.; Vasilakakis, M. Physiological and proteomic approaches to address the active role of ozone in kiwifruit post-harvest ripening. *J. Exp. Bot.* **2012**, *63* (7), 2449−2464.

(20) Kim, S.; Jeong, G. H.; Kim, S.-W. Ethylene Gas Decomposition Using ZSM-5/WO_3-Pt-Nanorod Composites for Fruit Freshness. *ACS Sustainable Chem. Eng.* **2019**, *7* (13), 11250−11257.

(21) Riahi, Z.; Ezati, P.; Rhim, J.-W.; Bagheri, R.; Pircheraghi, G. Cellulose Nanofiber-Based Ethylene Scavenging Antimicrobial Films Incorporated with Various Types of Titanium Dioxide Nanoparticles to Extend the Shelf Life of Fruits. *ACS Appl. Polym. Mater.* **2022**, *4* (7), 4765−4773.

(22) Riahi, Z.; Priyadarshi, R.; Rhim, J.-W.; Hong, S.-I.; Bagheri, R.; Pircheraghi, G. Titania Nanotubes Decorated with Cu(I) and Cu(II) Oxides: Antibacterial and Ethylene Scavenging Functions To Extend the Shelf Life of Bananas. *ACS Sustainable Chem. Eng.* **2021**, *9* (19), 6832−6840.
(23) Siripatrawan, U.; Kaewklin, P. Fabrication and characterization of chitosan-titanium dioxide nanocomposite film as ethylene scavenging and antimicrobial active food packaging. *Food Hydrocolloids* **2018**, *84*, 125−134.
(24) Xu, J.; Wang, F.; Zhan, J.; Li, Y.; Wang, T.; Ma, R.; Tian, Y. Construction of TiO_2/starch nanocomposite cryogel for ethylene removal and banana preservation. *Carbohyd. Polym.* **2023**, *312*, 120825.
(25) Gaikwad, K. K.; Singh, S.; Negi, Y. S. Ethylene scavengers for active packaging of fresh food produce. *Environ. Chem. Lett.* **2020**, *18* (2), 269−284.
(26) Ramacharyulu, P. V. R. K.; Muhammad, R.; Praveen Kumar, J.; Prasad, G. K.; Mohanty, P. Iron phthalocyanine modified mesoporous titania nanoparticles for photocatalytic activity and CO_2 capture applications. *Phys. Chem. Chem. Phys.* **2015**, *17* (39), 26456−26462.
(27) Roy, S.; Ramakrishnan, R.; Goksen, G.; Singh, S.; Łopusiewicz, Ł. Recent progress on UV-light barrier food packaging films − a systematic review. *Innovative Food Sci. Emerging Technol.* **2024**, *91*, 103550.
(28) Asjad, M.; Arshad, M.; Zafar, N. A.; Khan, M. A.; Iqbal, A.; Saleem, A.; Aldawsari, A. An intriguing case of morphology control and phase transitions in TiO_2 nanostructures with enhanced photocatalytic activity. *Mater. Chem. Phys.* **2021**, *265*, 124416.
(29) Han, X.; Kuang, Q.; Jin, M.; Xie, Z.; Zheng, L. Synthesis of Titania Nanosheets with a High Percentage of Exposed (001) Facets and Related Photocatalytic Properties. *J. Am. Chem. Soc.* **2009**, *131* (9), 3152−3153.
(30) Yu, J.; Low, J.; Xiao, W.; Zhou, P.; Jaroniec, M. Enhanced Photocatalytic CO_2-Reduction Activity of Anatase TiO_2 by Coexposed {001} and {101} Facets. *J. Am. Chem. Soc.* **2014**, *136* (25), 8839−8842.
(31) Asahi, R.; Morikawa, T.; Ohwaki, T.; Aoki, K.; Taga, Y. Visible-Light Photocatalysis in Nitrogen-Doped Titanium Oxides. *Science* **2001**, *293* (5528), 269−271.
(32) Foo, C.; Li, Y.; Lebedev, K.; Chen, T.; Day, S.; Tang, C.; Tsang, S. C. E. Characterisation of oxygen defects and nitrogen impurities in TiO_2 photocatalysts using variable-temperature X-ray powder diffraction. *Nat. Commun.* **2021**, *12* (1), 661.
(33) Livraghi, S.; Paganini, M. C.; Giamello, E.; Selloni, A.; Di Valentin, C.; Pacchioni, G. Origin of Photoactivity of Nitrogen-Doped Titanium Dioxide under Visible Light. *J. Am. Chem. Soc.* **2006**, *128* (49), 15666−15671.
(34) Cao, H.; Liu, F.; Tai, Y.; Wang, W.; Li, X.; Li, P.; Zhao, H.; Xia, Y.; Wang, S. Promoting photocatalytic performance of TiO_2 nanomaterials by structural and electronic modulation. *Chem. Eng. J.* **2023**, *466*, 143219.
(35) Xie, W.; Li, R.; Xu, Q. Enhanced photocatalytic activity of Se-doped TiO_2 under visible light irradiation. *Sci. Rep.* **2018**, *8* (1), 8752.
(36) Zhao, Y.; Li, C.; Liu, X.; Gu, F.; Du, H. L.; Shi, L. Zn-doped TiO_2 nanoparticles with high photocatalytic activity synthesized by hydrogen−oxygen diffusion flame. *Appl. Catal., B* **2008**, *79* (3), 208−215.
(37) Jiang, K.; Zhang, J.; Luo, R.; Wan, Y.; Liu, Z.; Chen, J. A facile synthesis of Zn-doped TiO_2 nanoparticles with highly exposed (001) facets for enhanced photocatalytic performance. *RSC Adv.* **2021**, *11* (13), 7627−7632.
(38) Pang, S.; Huang, J.-G.; Su, Y.; Geng, B.; Lei, S.-Y.; Huang, Y.-T.; Lyu, C.; Liu, X.-J. Synthesis and Modification of Zn-doped TiO_2 Nanoparticles for the Photocatalytic Degradation of Tetracycline. *Photochem. Photobiol.* **2016**, *92* (5), 651−657.
(39) Su, C.-Y.; Wang, L.-C.; Liu, W.-S.; Wang, C.-C.; Perng, T.-P. Photocatalysis and Hydrogen Evolution of Al- and Zn-Doped TiO_2 Nanotubes Fabricated by Atomic Layer Deposition. *ACS Appl. Mater. Interfaces* **2018**, *10* (39), 33287−33295.
(40) Parashar, M.; Shukla, V. K.; Singh, R. Metal oxides nanoparticles via sol−gel method: A review on synthesis, characterization and applications. *J. Mater. Sci.: Mater. Electron.* **2020**, *31* (5), 3729−3749.
(41) Gao, Y.; Masuda, Y.; Koumoto, K. Micropatterning of TiO_2 Thin Film in an Aqueous Peroxotitanate Solution. *Chem. Mater.* **2004**, *16* (6), 1062−1067.
(42) Varadharajan, K.; Singaram, B.; Mani, R.; Jeyaram, J. Enhanced Visible Light Photocatalytic Activity of Ag and Zn Doped and Codoped TiO_2 Nanoparticles. *J. Clust. Sci.* **2016**, *27* (5), 1815−1829.
(43) El-Desoky, M. M.; Morad, I.; Wasfy, M. H.; Mansour, A. F. Synthesis, structural and electrical properties of PVA/TiO_2 nanocomposite films with different TiO_2 phases prepared by sol−gel technique. *J. Mater. Sci.: Mater. Electron.* **2020**, *31* (20), 17574−17584.
(44) Spurr, R. A.; Myers, H. Quantitative Analysis of Anatase-Rutile Mixtures with an X-Ray Diffractometer. *Anal. Chem.* **1957**, *29* (5), 760−762.
(45) Byrne, C.; Moran, L.; Hermosilla, D.; Merayo, N.; Blanco, Á.; Rhatigan, S.; Hinder, S.; Ganguly, P.; Nolan, M.; Pillai, S. C. Effect of Cu doping on the anatase-to-rutile phase transition in TiO_2 photocatalysts: Theory and experiments. *Appl. Catal., B* **2019**, *246*, 266−276.
(46) Patterson, A. L. The Scherrer Formula for X-Ray Particle Size Determination. *Phys. Rev.* **1939**, *56* (10), 978−982.
(47) Meaurio, E.; López-Rodríguez, N.; Sarasua, J. R. Infrared Spectrum of Poly(l-lactide): Application to Crystallinity Studies. *Macromolecules* **2006**, *39* (26), 9291−9301.
(48) Wu, D.; Huang, A.; Fan, J.; Xu, R.; Liu, P.; Li, G.; Yang, S. Effect of blending procedures and reactive compatibilizers on the properties of biodegradable poly(butylene adipate-co-terephthalate)/poly(lactic acid) blends. *J. Polym. Eng.* **2021**, *41* (2), 95−108.
(49) Saha, K. K.; Zude-Sasse, M. Estimation of chlorophyll content in banana during shelf life using LiDAR laser scanner. *Postharvest Biol. Technol.* **2022**, *192*, 112011.

https://doi.org/10.1021/acsomega.4c09138
ACS Omega 2025, 10, 2931−2939